ELSEVIER

Journal of Fluids and Structures 20 (2005) 217–234

JOURNAL OF FLUIDS AND STRUCTURES

www.elsevier.com/locate/jfs

On decoupled and fully-coupled methods for blade forced response prediction

S. Moffatt*, L. He

School of Engineering, University of Durham, Durham DH1 3LE, UK

Received 5 May 2004; accepted 24 October 2004

Abstract

Two highly efficient fully-coupled methods of predicting the resonant forced response of turbomachinery blades have been developed with the intention of increased computational efficiency over a decoupled method. The flow and structural equations are solved simultaneously, based on the frequency-domain nonlinear harmonic method and the modal reduction technique. By combining the aerodynamic forcing and damping calculations into a single analysis, the coupled solution at a single excitation frequency is approximately half that of the decoupled method. Significant flow–structure coupling effects were discovered, leading to a study into the impact of frequency shift on the fully-coupled solution. A case study on the NASA Rotor 67 transonic aero fan rotor shows a significant reduction in vibration amplitude for the fully-coupled solution due to the resonant frequency shift, caused by the aerodynamic added mass effect. Prompting the development of a novel resonance-tracking algorithm to solve the additional degree-of-freedom in resonant frequency, the increase in computational efficiency in the fully-coupled method is lost due to the need for multiple solutions. A study into the added mass effect and the implications on the coupled solution is undertaken and an evaluation is made between the use of decoupled and fully-coupled forced response systems. It is shown that the decoupled method can accurately predict the resonant vibration level from a single calculation at the natural frequency and is insensitive to frequency shift for lightly damped cases.

1. Introduction

It is becoming widely accepted that forced response analysis must be integrated into the design phase of modern turbomachinery blades for both aero-engine and industrial gas turbine sectors. Fluid flow through turbomachines is inherently unsteady, where strong periodic flow perturbations can cause high levels of blade vibration for certain unavoidable resonant conditions. In search of improved efficiency and reduced engine size, commercial pressures are demanding higher blade loading and closer axial spacing, consequently pushing the limits of aeromechanical performance and increasing the risk of high-cycle fatigue failure caused by excessive resonant blade stresses. Conventional design methodologies based on empirical design rules cannot confidently predict blade vibration levels and the assessment of vibration performance is achieved through thorough engine testing. With increasing demands on the aeromechanical performance of modern blades, the capability to quantify resonant vibration levels on a routine

*Corresponding author. Westland Helicopters Ltd., Rotor Aeromechanics, Box 231, Yeovil, BA20 2YB, UK.
Tel.: +44 1935 702756.
E-mail address: moffatts@whl.co.uk (S. Moffatt).

0889-9746/$ - see front matter © 2005 Elsevier Ltd. All rights reserved.
doi:10.1016/j.jfluidstructs.2004.10.012

basis during the design stage is becoming more apparent in order to avoid costly redesign when vibration problems are detected late in development.

Forced response prediction poses a challenging problem due to the complex interaction between the fluid flow and blade structure. Forced vibration is caused by incoming periodic flow disturbances passing through the blade passages, resulting in an unsteady pressure field around the blade. Primarily arising from nonuniform inlet flow and wakes from upstream blades, resonant vibration occurs when the disturbance frequency closely matches the natural frequency of the blade structure. Consequently, the vibration of the blade induces a local unsteady pressure field in the surrounding fluid, resulting in aerodynamic damping and limiting the amplitude of vibration for forced response cases. Due to the high level of computation required by unsteady computational fluid dynamics (CFD) codes, routine forced vibration analysis remains prohibitively expensive for most manufacturers. Forced response prediction systems are categorized into either decoupled or fully coupled methods, which vary in the level of interaction between the fluid and structure.

Fully-coupled time-marching schemes combine the aerodynamic forcing and damping calculations, which are coupled together with the structural equations. The level of integration can vary from partially-integrated schemes, where the fluid and structural domains are solved separately with an exchange of boundary conditions at each step, to fully-integrated schemes, where the fluid and structural equations are solved simultaneously under the same numerical scheme. Fully-coupled methods based on both inviscid and viscous flow solvers have been used for flutter calculations by Marshall (1996), Gerolymos (1993), Silkowski et al. (2001) and Srivastava (2002). Advanced methods for forced response prediction combine sophisticated 3-D viscous multi-stage models with the modal reduction technique (Sayama et al., 2000; Bréard et al., 2000). Whilst reduced-order modelling techniques are normally adopted to reduce the computation of the finite element (FE) model, the computing efficiency of aeroelastic calculations is generally limited by the high computational demands of 3-D unsteady flow solvers. The need for fully 3-D calculations around vibrating blades has often been reported, such as shown by Bell and He (2000). Computational demands are generally too high for routine use due to the requirement for high temporal resolution and multi-passage or whole-annulus domains.

Linearized decoupled forced response methods provide a highly efficient frequency-domain approach, usually based on the linear solution of the 3-D Euler equations (Giles, 1992; Hall et al., 1994). Decoupled approaches calculate the aerodynamic forcing and damping independently before applying the aerodynamic forces to the structural equations. The approach is based on the assumptions of linear aerodynamic damping and that mode shapes are not affected by aerodynamic loading. These assumptions are generally valid for turbomachinery blades which are of high density and stiffness and vibrate at low amplitudes. Aerodynamic damping is calculated based on the projection of the blade mode-shape onto the fluid mesh, where the solid boundary of the passage is set to vibrate with fixed amplitude and mode-shape. The resulting vibration-induced pressures are directly or indirectly scaled in a linear fashion to represent aerodynamic damping. It is commonly accepted that mode-shapes effectively remain unchanged for lightly-damped turbomachinery blades, and this assumption has been widely adopted (Kielb, 1999; Marshall and Imregun, 1996). Linear aerodynamic damping behaviour for two transonic fan rotors has been observed by Li and He (2002), and Schmitt et al. (2003). Linear flow solvers combined with the decoupled method have been reported for both resonant (Kielb, 1999; Chiang and Kielb, 1993; Manwaring and Kirkeng, 1997; Campobasso and Giles, 2000), and transient forced vibration problems (Green and Marshall, 1999). The use of nonlinear time-marching schemes with the decoupled method, although less common, has been reported by Schmitt et al. (2003) and Moyroud et al. (2000).

The nonlinear harmonic method has been used for decoupled forced response calculations by Moffatt and He (2003) to provide a frequency-domain approach capable of dealing with flow nonlinearities that is typically 30–100 times faster than equivalent multi-passage time-marching calculations (Ning et al., 2003a,b; Chen et al., 2001). Whilst this decoupled method is a linearized approach, it is not restricted to linear flow conditions. Since aerodynamic forcing terms are vibration-independent, flow nonlinearities remain decoupled from blade motion and are therefore handled intrinsically. For cases where aerodynamic damping is suspected to be nonlinear, the damping calculation can simply be restarted at the solution vibration amplitude without a large gain in total CPU time. However, there has not yet been any reported evidence showing significant nonlinear damping under typical forced response conditions. Two distinct approaches to the solution of the decoupled forced response equation are based on the principles of (a) equivalent viscous aerodynamic damping (Moffatt et al., 2003); and (b) superposition of aerodynamic forces (Schmitt et al., 2003).

Decoupled and coupled aeroelastic methods have been developed fairly independently within the disciplines of linearized and time-accurate CFD and few comparative studies have been published (Schmitt et al., 2003; Tran et al., 2003; Marshall et al., 2000). Schmitt et al. show that the aerodynamic forces of the coupled solution closely match the superimposed decoupled forces for a counter-rotating prop fan, and Tran et al. show agreement between a variety of coupled and decoupled methods when calculating the aeroelastic stability of a transonic blade row. However, no consideration is made in either paper for the decoupled approach based on viscous aerodynamic damping.

In this paper, the decoupled approach of Moffatt and He is further developed into two fully-coupled methods based on the nonlinear harmonic method. Blade vibration is modelled with a single degree-of-freedom (DoF) modal equation

on the CFD mesh and solved simultaneously with the flow equations. The modal equation is solved numerically in both the frequency and time-domains, directly coupling with the flow equations at each solution step. A novel resonance tracking scheme is implemented to capture the resonant frequency shift of the coupled solution, resulting from the added mass effect of fluid structure coupling. A study on the implications of the added mass effect on the coupled solution is presented, with modelling of fluid inertial forces provided by an adapted approach to the decoupled solution. The paper is concluded with an evaluation on the use of coupled and decoupled forced response methods for various turbomachinery applications.

2. Overview of decoupled system

Described in detail by Moffatt and He (2003), and illustrated in Fig. 1, the decoupled method represents an open-loop system, requiring only a single execution of the fluid and structural equations. Resonant vibration of a single mode is considered, with aerodynamic excitation provided by periodic aerodynamic disturbances occurring at the blade natural frequency, subject to aerodynamic and mechanical damping. Blade mode shapes and natural frequencies are provided by a modal analysis of a FE model of the blade structure using the commercial FE solver, ANSYS. The mode of interest is selected from the Campbell diagram, and then interpolated onto the CFD mesh. The CFD analysis is performed in two separate parts: (a) aerodynamic excitation pressures due to bladerow interaction or inlet distortion calculated through passages with rigid blades, providing the modal excitation force; and (b) induced damping pressures calculated with a fixed amplitude of blade vibration in an isolated bladerow to yield the aerodynamic damping ratio. The aerodynamic force distributions from the two calculations are transformed from the physical domain into the modal domain, based on the fluid mesh. The forced response analysis involves the analytical solution of the modal equation to provide the modal amplitude, which is then expanded to provide absolute blade displacements and oscillating blade stresses at the resonant condition on either the CFD or FE mesh.

2.1. CFD method

The nonlinear harmonic method has been developed in order to predict unsteady flow in turbomachinery caused by bladerow interaction (Chen et al., 2001) and blade vibration (Vasanthakumar et al., 2000). The 3-D unsteady viscous flow is linearized by superimposing harmonic perturbations onto a time-averaged flow then solved in the frequency-domain using a pseudo-time marching scheme. Only the fundamental flow harmonic is considered for the present aeromechanical analysis, assuming that higher pressure harmonics do not affect the steady-state blade vibration. Nonlinearity can be included by solving the time-averaged and unsteady perturbation equations in a coupled manner, where the deterministic stress terms of the time-averaged flow are influenced by the flow unsteadiness. A single passage approach is adopted, and the governing equations are solved in the frequency domain, hence avoiding the need for high temporal resolution and leading to significant gains in computational efficiency over conventional multi-passage time-marching schemes. Aerodynamic forcing is provided by a multi-stage calculation through passages with nonvibrating

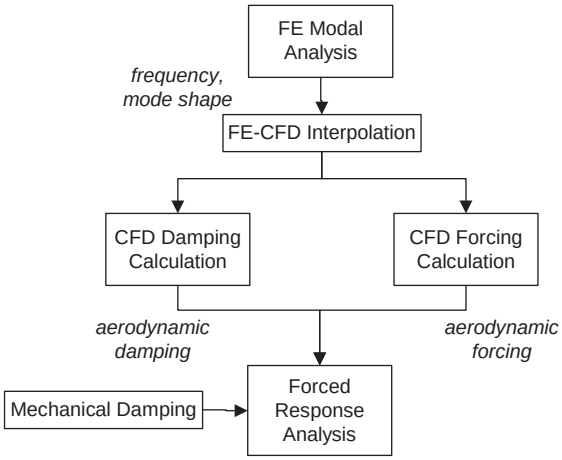

Fig. 1. Decoupled system.

blades to provide the complex harmonic force distribution acting on the blade due to the effects of bladerow interaction or inlet distortion. The damping forces are obtained from a single bladerow calculation with undistorted inlet flow and the blade is set to vibrate in the specified mode with a fixed realistic amplitude. The damping forces are integrated over one vibratory cycle to give the work done on the blade, which can be scaled to provide an absolute damping value for any given blade vibration amplitude.

2.2. Structural modelling

The resonant vibration of a single mode is modelled using modal reduction theory, which reduces the number of coupled dynamic equations of a FE model of j DoF to a single-DoF modal equation. Modal reduction is often used in aeromechanical analysis, and it is generally accepted that resonant vibration can be modelled with a single equation for most situations. The modal equation

$$m\ddot{q} + 2\zeta\omega_n m\dot{q} + kq = f \tag{1}$$

is solved for a given total damping ratio $\zeta = \zeta_{\text{aero}} + \zeta_{\text{mech}}$ to give the modal amplitude, q. To simplify computation, the mode eigenvector is normalized to unity modal mass, m, and a modal stiffness of $k = \omega_n^2$. Assuming harmonic motion at the forcing frequency under harmonic loading and letting $q = \tilde{q}e^{i\omega t}$ and $f = \tilde{f}e^{i\omega t}$, where $i^2 = -1$, the harmonic force amplitudes acting on the blade surface are transformed into modal coordinates by taking the dot product of the real eigenvector, $\{\phi\}$, and the complex force vectors using

$$\tilde{f} = \sum_{j=1}^{n} \{\phi_j (F^{\text{Real}} + iF^{\text{Imag}})_j\}, \tag{2}$$

$$\tilde{d} = \sum_{j=1}^{n} \{\phi_j (D^{\text{Real}} + iD^{\text{Imag}})_j\}, \tag{3}$$

to yield the complex modal excitation force, $\tilde{f}$, and the modal damping force, $\tilde{d}$, from the physical complex force vectors $\{\tilde{F}\}$ and $\{\tilde{D}\}$ from the CFD forcing and damping calculations. The complex damping force induced by the blade motion is assumed to increase linearly with modal amplitude, and with constant phase relative to the blade motion. This allows aerodynamic damping to be considered as a damping ratio based on the principle of equivalent viscous damping, given by

$$\zeta_{\text{aero}} = \frac{-W_d^{\text{cfd}}}{2\pi\omega^2 (q^{\text{cfd}})^2}, \tag{4}$$

where W_d^{cfd} is the work done on the blade per vibratory cycle in the CFD damping calculation at the specified vibration amplitude q^{cfd}. With mechanical damping also expressed as an equivalent damping ratio, ζ_{mech}, the solution of the modal equation is given by

$$\tilde{q} = \frac{\tilde{f}}{(\omega_n^2 - m\omega^2) + i(2\{\zeta_{\text{aero}} + \zeta_{\text{mech}}\} m\omega_n\omega)} \tag{5}$$

to yield the modal amplitude. Absolute blade displacements are given by scaling the mass-normalized eigenvector by the modal amplitude.

3. Fully-coupled systems

Two fully-coupled methodologies have been developed that simultaneously solve the modal and fluid equations within the flow solver. By combining the aerodynamic damping and forcing parts into a single calculation, the coupled methods were developed with the intention of halving the solution time. Based on the frequency-domain nonlinear harmonic unsteady aerodynamic solution, two approaches are presented based on the solution of the modal equation in both the frequency-domain and the time-domain. Due to the combined excitation and damping forces in the coupled solution, the coupled modal equation is modified such that the aerodynamic forces are superimposed on the right-hand side of the equation,

$$\ddot{q} + 2\zeta_{\text{mech}}\omega\dot{q} + \omega^2 q = f + d(q), \tag{6}$$

thus separating mechanical and aerodynamic terms. Since the mechanical and aerodynamic terms on each side of the equation are now dependent on the blade response, the equation is solved in an iterative manner until convergence is reached between the structural and aerodynamic domains. At each step of the solution, harmonic force and displacement amplitudes are exchanged between the modal and fluid equations, all of which are solved using a 4-stage Runge–Kutta scheme. The modal amplitude effectively becomes an additional DoF in the fluid solution with close coupling between the fluid and structure.

3.1. Frequency-domain solution

Both the fluid and modal equations are solved in the frequency-domain by pseudo-time marching with an exchange of information after each step, as shown in Fig. 2. Assuming harmonic motion and forcing and representing modal velocity as $v = \dot{q}$, the modal equation (1) can be represented by the two equations

$$\tilde{v} = \mathrm{i}\omega\tilde{q} \text{ and } (2\zeta_m\omega_n + \mathrm{i}\omega)\tilde{v} + \omega_n^2\tilde{q} = (\tilde{f} + \tilde{d}(q)), \tag{7}$$

where the complex damping force

$$\tilde{d}_n(q) = \tilde{q} \times \frac{\tilde{d}^{\mathrm{cfd}}}{q^{\mathrm{cfd}}} = \tilde{q} \times (d_n^{\mathrm{real}} + \mathrm{i}d_n^{\mathrm{imag}}) \tag{8}$$

is directly scaled by the modal amplitude. Introducing the pseudo-time derivatives $R_q = \partial\tilde{q}/\partial\tau$ and $R_v = \partial\tilde{v}/\partial\tau$, and letting

$$\tilde{a}_q = \mathrm{i}\omega \text{ and } \tilde{a}_v = 2\zeta_m\omega_n + \mathrm{i}\omega, \tag{9}$$

the 4-stage Runge–Kutta equations are obtained from

$$R_q^n = \tilde{v}^n - \tilde{a}_q\tilde{q}^n, \tag{10}$$

$$R_v^n = (\tilde{f} + \tilde{d}(q)) - \tilde{a}_v\tilde{v}^n - \omega^2\tilde{x}^n \quad (n = 0, 1, 2, 3). \tag{11}$$

When the pseudo-time marching solution has converged, the left-hand sides of Eq. (10) and Eq. (11) disappear, recovering the original modal equation and definition of velocity.

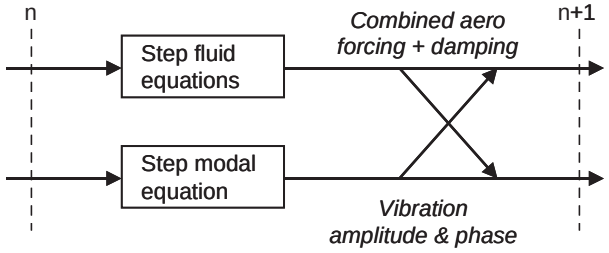

Fig. 2. Frequency-domain fully-coupled system.

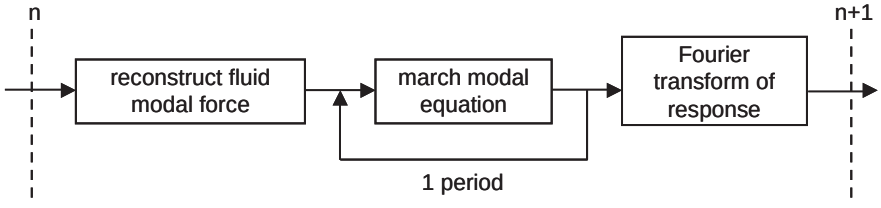

Fig. 3. Time-marching of modal equation.

3.2. Time-marching of modal equation

An alternative hybrid approach is based on the continuous time-domain solution of the modal equation with periodic updating of the aerodynamic modal force. As shown in Fig. 3, flow–structure interaction is dealt with in an identical manner to the previous approach, exchanging the modal force and amplitude at each step. Reconstructing one period of the current harmonic modal force amplitude at each solution step, the modal equation is time-marched using the 4-stage Runge–Kutta scheme for one period. A Fourier transform of the modal response over the period provides the updated harmonic modal amplitude at the forcing frequency.

The coupled methods require the modal equation to converge at a similar rate to the flow equations in order to avoid instability and maintain computing efficiency. Instability occurs when the modal equation converges at a faster rate than the fluid, where the aerodynamic damping forces cannot respond to the blade motion. Under such conditions, the unresponsive damping force will effectively cause further blade excitation and the motion will tend to incorrectly lag the combined aerodynamic force by 90° with excessive amplitude, until the flow equations react accordingly. A high degree of oscillation will occur and the solution will diverge. A slow modal convergence rate will be very stable but with a large detriment to solution efficiency. For the frequency-domain solution of the modal equation, the convergence rate is tuned by adjusting the pseudo-time step size, which is determined independently of the flow equations. In the hybrid approach, stability is ensured by smoothing the updated modal amplitude at each solution step. Convergence can be accelerated by increasing the number of periods the modal equation is marched per solution step.

4. Comparative study and discussion

4.1. Comparison of coupled and decoupled solutions

The NASA Rotor 67 transonic fan rotor is used as a test case to provide a comparison of the coupled and decoupled forced response methods. Previous publications by other authors on the aeromechanical analysis of NASA Rotor 67 have included the flutter calculations of Marshall (1996) and Srivastava et al. (2002), based on time-accurate CFD codes. In this paper, blade natural frequencies and mode shapes are calculated from the FE model using typical properties for titanium and accounting for the centrifugal blade loading. Comprising of 806 20-node brick elements, the blade is modelled with the aerofoil cantilevered at the hub, due to the lack of root data. The linear Navier–Stokes equations are solved on a single-passage H-mesh of $110 \times 25 \times 29$ density. Both the FE and CFD meshes are shown in Fig. 4, together with a contour plot of the mode 7 mode-shape. A blade count of 21 was used in order to compare results with previous work. The coupled and decoupled solutions of modes 1, 2, 3 and 7 are presented to provide forced response studies typical of inlet distortion and bladerow interaction problems. Blade excitation is provided by hypothetical inlet distortions with the number of nodal diameters chosen to provide resonant forcing at a frequency close to design speed. Inlet flow conditions are based on the steady solution close to design load, where the inlet flow perturbation is determined by specifying the amplitude of variation in axial velocity, V_x, and applying a variation in density to ensure isentropic inlet conditions. The rotor geometry and the 2-node inlet distortion are illustrated in Fig. 5 and a summary of the resonant conditions is provided in Table 1.

Fig. 6 shows the well-matched convergence history of the combined aerodynamic modal force ($f + d$) and the modal amplitude of the coupled calculation for mode 1 at natural frequency. The forced response predictions given by the coupled and decoupled methods at the blade natural frequencies without mechanical damping are listed in Table 2. The solution amplitudes are expressed in terms of the absolute blade vibration amplitude at the tip leading edge, normalized by chord length. Whilst a very high level of agreement was found between the two coupled methods, the responses predicted by the coupled solutions of all modes were found to be significantly lower than the decoupled solutions. By repeating the coupled calculations at frequencies around the natural frequency (Fig. 7), it can be observed that the coupled solution is subject to a frequency shift. However, the solution of the decoupled Eq. (5) does not show any frequency shift. Whilst the decoupled solution encounters resonance at the natural frequency, the coupled solution is excited slightly off-resonance and, hence, experiences a lower amplitude of vibration. The peak amplitudes given by the coupled and decoupled methods at their respective frequencies can be seen to agree very closely. It is evident that both methods are capable of predicting peak forced vibration levels with a high level of agreement, providing that the coupled calculation is performed at the correct frequency. Whereas the decoupled calculation is solved at the blade natural frequency, the resonant frequency of the coupled solution is unknown and must be found to avoid under-predicting the response at an off-resonant condition.

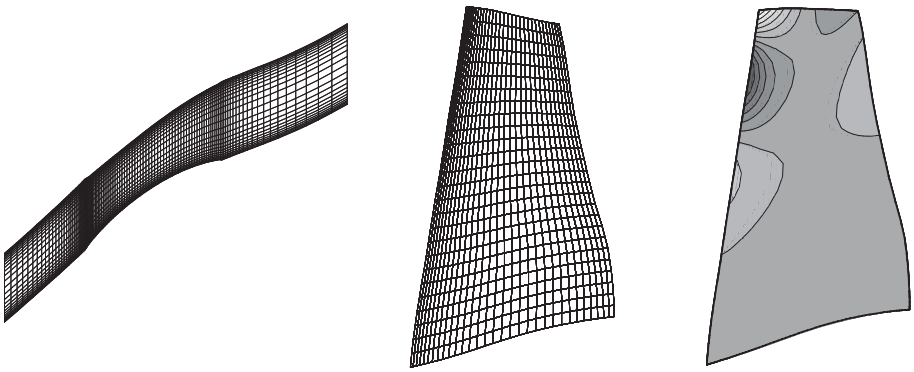

Fig. 4. CFD mesh, FE mesh and mode 7 mode-shape.

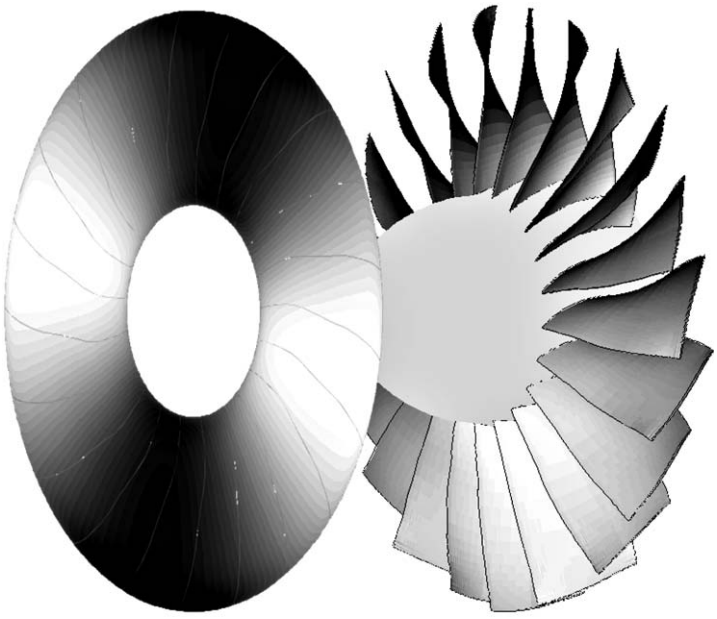

Fig. 5. Fan geometry and 2-node inlet distortion.

Table 1
Resonant conditions

Mode no.	Mode type	Frequency (Hz)	Number of nodal diameters	V_x distortion amplitude (%)
1	1st bend	601.0	2	1
2	2nd bend	1307.9	5	5
3	1st torsion	1913.2	7	15
7	Combined	4198.4	15	15

The dependency on solution frequency creates an additional DoF into the coupled calculation, which cannot be obtained directly from the governing equations. As discussed later in this paper, the resonant frequency cannot be calculated from a coupled solution at any one frequency, due to the lack of information that can be obtained from the combined aerodynamic force. Instead, the coupled solution must be repeated at a number of discrete frequencies around the resonant peak to reveal the frequency response curve, which can be done with an open-loop frequency sweep or by implementing a closed-loop resonance tracking algorithm. Whilst the fully coupled method models the physical system in a more realistic manner, this case suggests that a higher degree of modelling is required to include the effects

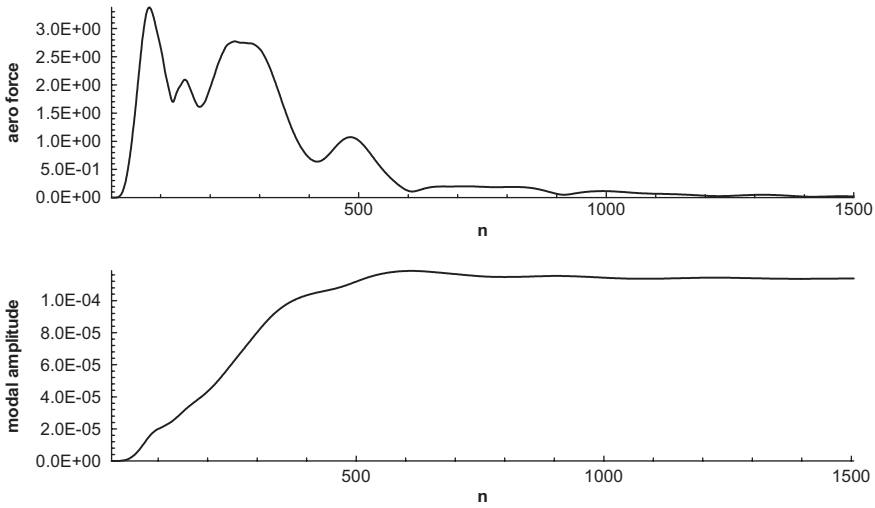

Fig. 6. Convergence of coupled solution for mode 1 at natural frequency.

Table 2
Decoupled and coupled response predictions

Mode no.	Decoupled	Coupled (freq. domain)	Coupled (hybrid)	
	Tip L.E. Amp. (% chord)	Tip L.E. Amp. (% chord)	Tip L.E. Amp. (% chord)	Response drop (%)
1	1.096	0.949	0.949	13.81
2	0.691	0.628	0.628	8.03
3	0.521	0.498	0.498	4.37
7	0.164	0.116	0.116	29.03

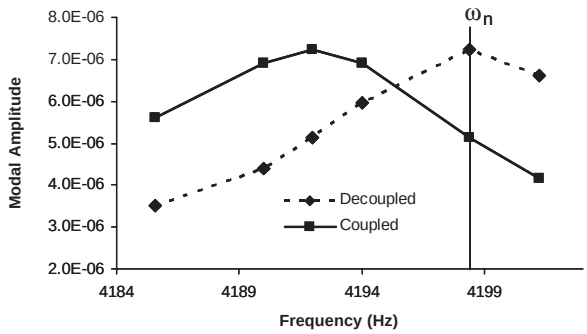

Fig. 7. Coupled and decoupled solutions around resonant peaks for mode 7.

of the additional phenomena captured in the analysis. The sources of the frequency shift and the implications on the coupled method are now discussed in detail.

4.2. Resonance tracking

An efficient resonance tracking scheme was implemented to direct the solution towards the resonant frequency, hence avoiding the excessive computation of a frequency sweep. Exploiting the fact that the frequency-domain fluid solution

can be efficiently restarted at a new frequency, the scheme was developed with the intention of minimising computing time. By approximating portions of the bell-shaped frequency response curve by the parabola

$$a\omega^2 + b\omega + c = q, \tag{12}$$

it is possible to accurately predict the resonant frequency with a small number of iterations. Starting with the coupled solution at the blade natural frequency, the solution is then restarted twice to obtain a further two solutions at frequencies close to the natural frequency. Fitting a parabolic curve to the three points on the response curve enables an estimate of the resonant frequency, as shown in Fig. 8. Depending where the three points lie on the response curve, the quadratic coefficient, a, of the parabola will be either positive or negative. Negative values result in an upturned parabola approximating the top of the bell-shaped response curve close to the resonant peak. This allows the resonant frequency to be accurately predicted by simply calculating the stationary point of the curve, giving the frequency corresponding at the peak. If desired, the solution can be repeated at the predicted peak to verify convergence in frequency. Positive values of the quadratic coefficient, however, approximate the lower parts of the bell-shaped response curve at frequencies either above or below the resonant peak. Here, the stationary point will not correspond to the resonant peak and an iteration in solution frequency is required. In this situation, the solution frequency is updated by a pre-defined step size, with the step direction being determined by comparing the response amplitudes of the solutions. The coupled solution is restarted at the new frequency and a new parabola is calculated using the latest three frequencies. The frequency updating is repeated until a negative parabola is achieved and the resonant peak can be calculated at the stationary point. In order to speed up convergence, the frequency step size is reduced if oscillation in solution frequency is detected. This allows a relatively large initial frequency step be specified, which is then automatically reduced in the eventuality that the algorithm overshoots the natural frequency.

The fully-coupled solution with resonance tracking was performed for mode 3, giving a frequency shift of 3.5 Hz and peak amplitude at tip L.E. of 1.098% chord. Using an initial step size of 1 Hz and a step reduction factor of 0.4, convergence in frequency was achieved after six solutions with total computing time being approximately double that of a single complete coupled calculation. It has been demonstrated that the coupled method will under-predict resonant vibration levels unless a frequency sweep or resonance tracking scheme is implemented. The coupled and decoupled solutions will agree only when the coupled analysis is performed at the resonant frequency, which is found by repeating the coupled calculation for a range of frequencies. The need for resonance tracking increases the overall computational effort of the coupled solution, where the gain in efficiency of a single solution over the decoupled approach is lost.

4.3. Fluid–structure coupling effects

The principles behind the coupling effect are now discussed to identify the main source of the frequency shift and provide a basis to evaluate the impact on coupled and decoupled methods. The obvious impact on the coupled solution is the additional computation of the resonance tracking to avoid under-prediction at the natural frequency. Whilst a single coupled calculation is preferable, the need for resonance tracking is determined by the level of agreement between a single coupled calculation at the natural frequency and the resonant peak. An understanding of the source of frequency shift provides an insight into the factors affecting the sensitivity of the coupled solution to frequency shift. In addition, the modelling of the coupling effect allows the accuracy of the decoupled approach to be assessed.

The difference in behaviour between the decoupled and fully-coupled methods is due to a fluid–structure coupling effect present in the coupled solution resulting from the aerodynamic damping forces. For a specific blade motion, the

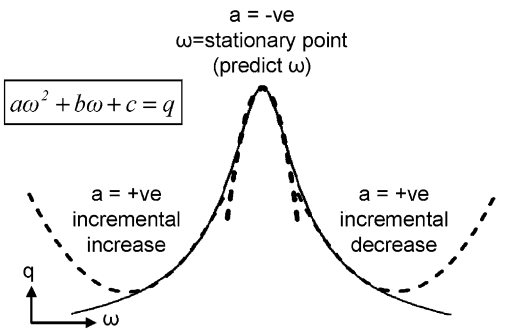

Fig. 8. Resonance tracking using parabolic curve fitting.

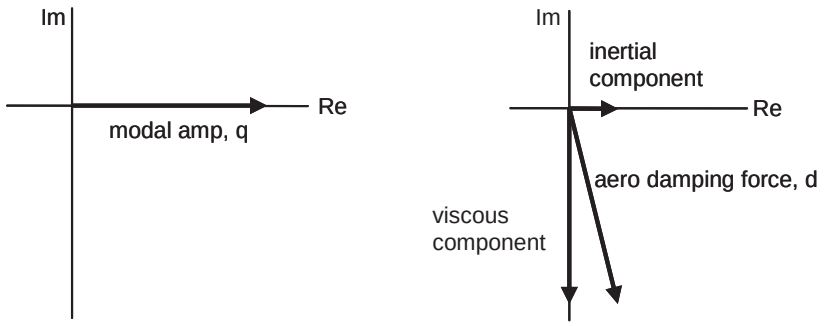

Fig. 9. Argand diagram of vibration-induced complex modal damping force.

induced pressures acting on the blade result in a modal damping force which lags the blade motion for forced response cases (modal force will lead the motion for flutter cases), as illustrated on the Argand diagrams in Fig. 9. Here, a complex aerodynamic modal damping force is induced by a real modal amplitude. In a dynamic situation, the modal amplitude will vary in phase and magnitude and the damping force will lag by a fixed relative phase angle with the magnitude increasing in a linear manner, based on the assumption of linear aerodynamic damping. In the coupled solution, the real and imaginary damping force components have two distinct effects on the dynamic response of the system. Damping is provided solely by the imaginary (out-phase) force component due to the fact that no work can be done by the real (in-phase) component. However, the real component is aligned with the blade inertial forces, therefore, causing a variation of the blade dynamic mass. The result is an added mass effect, leading to a change in the dynamic resonant frequency. In this paper, the real and imaginary components are referred to as inertial and viscous components, respectively. The viscous component is named as such for the reason that it provides the viscous aerodynamic damping effect to the blade, and is not to be confused with the viscous fluid forces. The viscous and inertial components of the complex modal force are determined by the interaction of pressure fluctuations with the mode-shape and are not directly related to the viscous terms of the flow equations.

The decoupled method considers the damping force as an equivalent viscous damping ratio based on the damping work, as shown in Eq. (4). The inertial component of the damping force is subsequently neglected, removing the capability of the decoupled method to include the added mass effect. Since the dynamic mass of the system is unchanged, the decoupled solution does not experience any significant frequency shift. In contrast, the inertial and viscous components in the coupled solution cannot be identified due to the fact that excitation and damping forces are combined and cannot be separated. The added mass effect is therefore an integral part of the coupled solution.

An investigation into the coupling effect was carried out using an adapted version of the decoupled method to model the added mass effect based on the analytical solution of the coupled Eq. (6). To emulate the coupled solution, both the inertial and viscous components of the damping force are scaled by the modal amplitude, giving the analytical solution

$$\tilde{q} = \frac{\tilde{f}}{(\omega_n^2 - m\omega^2 - d_n^{\text{real}}) + \mathrm{i}(2\zeta_{\text{mech}} m\omega_n\omega - d_n^{\text{imag}})}. \tag{13}$$

This approach is equivalent to the 'superposition' approach discussed by Schmitt et al. (2003), which has been shown to closely resemble the coupled solution for typical cases without significant nonlinear damping characteristics. Based on the decoupled aerodynamic forces calculated at the blade natural frequency, the response curves are extrapolated around the resonant peak using Eqs. (5) and (12) to simulate the response of the coupled method and provide a comparison with the decoupled solution. A comparison of the two decoupled methods for mode 7 is given in Fig. 10, showing the resonant frequency shift. The extrapolated curves are compared with the fully-coupled solutions at a range of frequencies for each of the four modes in Fig. 11. It can be seen that the decoupled solution with added mass agrees very well with the coupled method, verifying the ability of the decoupled method to predict vibration levels at frequencies slightly different from the solution frequency. This is due to the fact that the aerodynamic solutions do not vary significantly over such a small frequency range; therefore, variation in vibration amplitude is caused primarily by blade structural dynamic effects.

For any single DoF forced oscillator, the phase angle at which the response will lag the excitation force will be very small for low frequencies and will approach 180° for high frequencies. At resonance, the response will lag the force by 90°, when the maximum work is applied to the blade. The response phase lag is very sensitive to frequency around the resonance and will change very quickly for small deviations around the resonant frequency. In Eq. (12) it can be seen

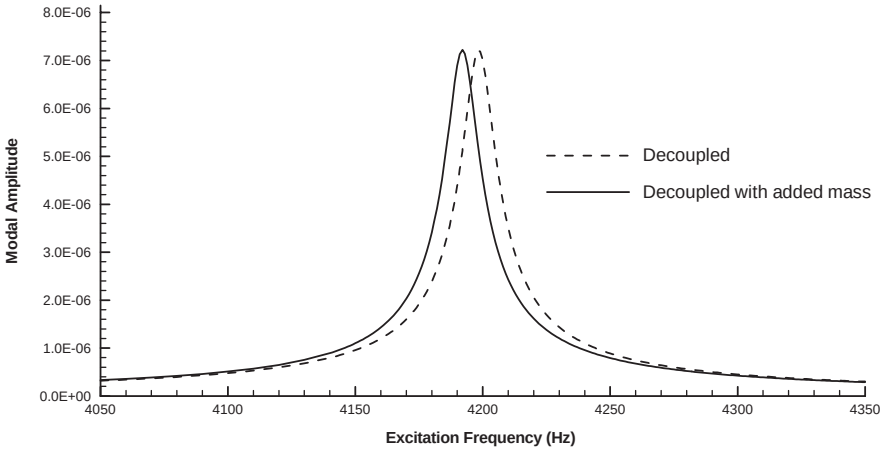

Fig. 10. Frequency response curves for mode 7.

that resonance occurs when the denominator is purely imaginary, hence, $\omega_n^2 - m\omega^2 - d_n^{\text{real}} = 0$ (where $m = 1$). This condition is only seen with excitation at the resonant frequency. The decoupled method simplifies the response solution by neglecting the d_n^{real} term, ensuring that the resonant condition of the 90° phase lag always occurs at the blade natural frequency.

Table 3 shows the high level of agreement between the resonant peaks of the decoupled and coupled solutions at their respective frequencies. The important point to note is that the exclusion of the added mass effect in the decoupled solution makes no significant difference in the resonant peak. This is due to the fact that the aerodynamic and structural dynamic behaviour does not vary significantly over such a narrow frequency range. Both aerodynamic excitation and damping forces were found to be insensitive to frequency within the ranges of the resonant peaks. In addition, Srivastava et al. (2002) reported that aerodynamic damping varied very little within a surprisingly large frequency range for the 1st bending mode of a transonic fan. In terms of structural dynamics, the resonant response amplitude for a given excitation source is determined by the level of total viscous damping, which is equal for both approaches. Regardless of whether or not added mass is included, the denominators of the forced response solution equations (5) and (12) reduce to $2\zeta m\omega_n\omega$ at resonance. Therefore, for a given damping ratio, the resonant response amplitude is inversely proportional to the frequency, which does not significantly vary over such a narrow range.

The flow–structure coupling effect can also have a reduced mass effect, resulting in a positive frequency shift as experienced by mode 1. In fluid–structure coupling applications, added mass is usually considered as a region of fluid attached to the moving solid boundary, which requires an inertial force to accelerate the attached fluid with the structure (Liu, 1994). It is evident that this interpretation does not hold for turbomachinery cases, which involve the high speed flow of low-density fluids with thin boundary layers and often include shock oscillation. The apparent inertial force results from the phase of the complex flow phenomena acting on the blade in relation to the mode-shape displacements, rather than the physical oscillation of an attached region of fluid. However, it is now shown that the vibration-induced aerodynamic force component which is in phase with the blade motion can be considered as an added (or reduced) mass for forced response analysis.

4.4. Decoupled prediction of frequency shift

It is now shown how a single decoupled solution can be used to accurately predict the resonant peak with the option of either including of disabling the blade added mass effect. An evaluation of the added mass effect and the implications of the frequency shift on the coupled solution is presented, starting with a comparison of the frequency shift due to viscous damping and the added mass effect. It is well known that the damped resonant frequency is given by

$$\omega_d = \omega_n\sqrt{1-\zeta^2}. \tag{14}$$

The dynamic resonant frequency due to the added mass effect alone is calculated by considering the added mass in terms of the inertial damping force component. From Eqs. (10) and (12), the modal equation is rewritten

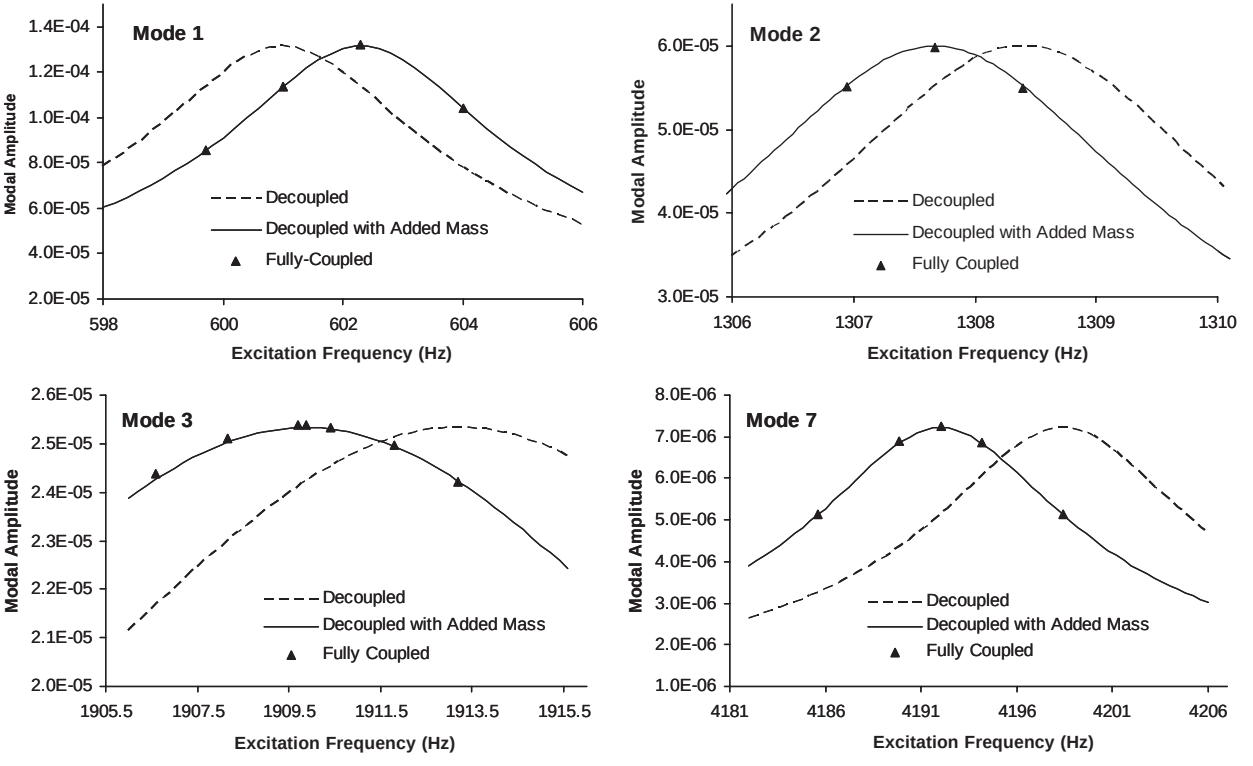

Fig. 11. Frequency response curves for coupled and decoupled calculations.

Table 3
Comparison of decoupled resonant peaks

Mode	Decoupled resonant peak		Coupled resonant peak	
	Frequency (Hz)	Tip L.E. amplitude (% chord)	Frequency (Hz)	Tip L.E. amplitude (% chord)
1	601.0	1.096	602.29	1.099
2	1307.9	0.691	1307.2	0.688
3	1913.2	0.521	1909.7	0.511
7	4198.4	0.164	4192.0	0.164

Table 4
Frequency shift due to viscous and inertial damping force components

Mode	Damped frequency shift, $\Delta\omega_d$ (Hz)	Dynamic frequency shift, $\Delta\omega_{\text{dyn}}$ (Hz)
1	−0.0041	+1.31
2	−0.0011	−0.728
3	−0.0309	−3.32
7	−0.00493	−6.383

in the form

$$\left\{-\omega^2\left(1+\frac{d_n^{\text{real}}}{\omega^2}\right)+\omega_n^2+\text{i}(2\zeta_{\text{mech}}\omega_n\omega-d_n^{\text{imag}})\right\}\tilde{q}=\tilde{f}. \tag{15}$$

It is evident that the dynamic mass, m', of the system at resonance can be given by the expression

$$m'=1+\frac{d_n^{\text{real}}}{\omega^2}. \tag{16}$$

The dynamic natural frequency, ω_{dyn}, is therefore given by

$$\omega_{\text{dyn}}=\sqrt{\frac{\omega_n^2}{m'}}, \tag{17}$$

where ω_n^2 is the modal stiffness. To avoid the simultaneous solution of Eqs. (16) and (17) at the unknown frequency, ω_{dyn}, the excitation frequency, ω, in Eq. (16) can be substituted for the blade natural frequency, ω_n, since the frequency shift is relatively low. Based on the decoupled damping calculation, the frequency shifts due to the viscous damping and added mass effects given by Eqs. (14) and (17) are compared for each of the four modes. The calculated frequency shifts for the four modes listed in Table 4 show that the added mass effect dominates the viscous damping effect by 2–3 orders of magnitude. It can therefore be deduced that the frequency shift can be considered to be solely due to the added mass effect.

In addition to forced response cases, the decoupled approach is equally capable of predicting the aeroelastic stability and frequency shift in flutter calculations. Whereas forced vibration levels are dependent on both the excitation forces provided by incoming aerodynamic disturbances and the vibration-induced damping forces, flutter stability is determined solely by the vibration-induced aerodynamic forces. Flutter stability can therefore determined by performing the decoupled damping calculation, where a positive value of aerodynamic damping provides stability and a negative value indicates instability. The damping calculation for mode 1 was repeated at interblade phase angles of 0°, 90°, 180° and −90° for comparison with the coupled and decoupled flutter predictions made by Marshall (1996). The predicted damping and frequency shift was in good agreement with the coupled and decoupled values predicted by Marshall for the 0° IBPA condition. Reasonable agreement was observed for the remaining three phase angles, accounting for the variation between the different solutions of Marshall.

4.5. Coupled prediction of frequency shift

Unlike the decoupled method, a single coupled calculation cannot be used to extrapolate the frequency response function; therefore, the resonant peak cannot be identified based on the solution at any one frequency. This is due to the fact that the aerodynamic excitation and damping forces are combined and cannot be separated, resulting in the need for multiple solutions to find the resonant frequency. The aerodynamic modal forces of the mode 3 solution are plotted on the Argand diagrams in Fig. 12, together with the response phase angles for a range of frequencies around resonance. For simplicity, no mechanical damping is present. To clarify the terminology, the damping force refers to the total vibration-induced aerodynamic force, consisting of the 'viscous' out-phase component and the 'inertial' in-phase component; the excitation force is due to incoming aerodynamic disturbances and is independent of blade motion; and the combined force is the sum of the aerodynamic damping and excitation forces. It can be seen that the excitation force

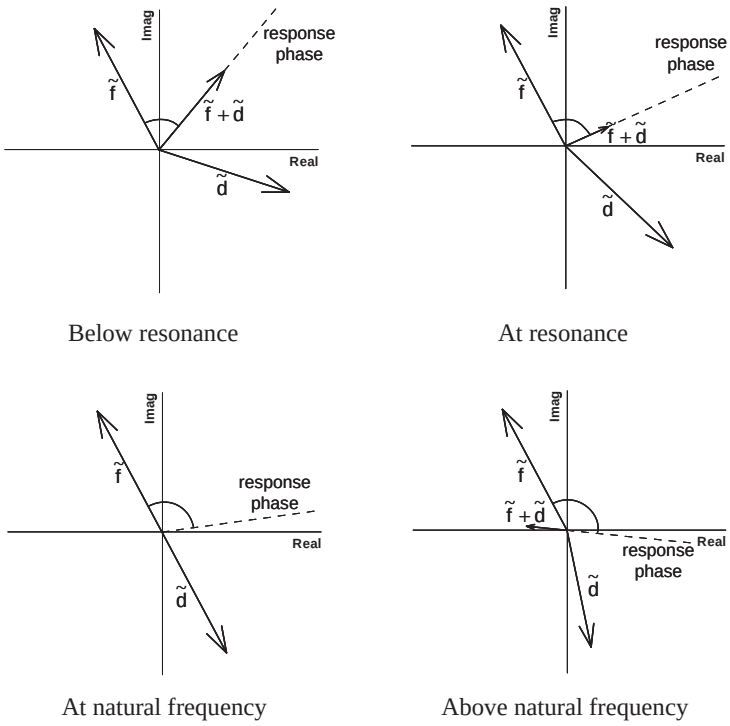

Fig. 12. Argand diagram of forces at solutions around resonant peak for mode 3.

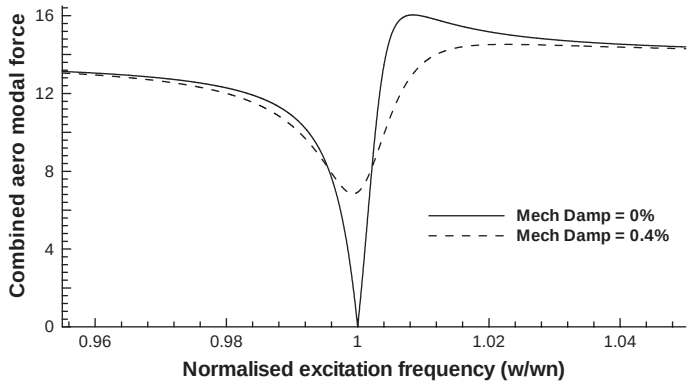

Fig. 13. Variation of combined aerodynamic force with excitation frequency for mode 1.

is held constant over the narrow resonant frequency range and the damping force lags the blade motion with constant relative phase. An important point to note is that the resulting combined aerodynamic force is zero only when solved at the natural frequency when no mechanical damping is present, at which point the aerodynamic damping force exactly balances the excitation force.

Fig. 13 shows the variation of the combined steady-state aerodynamic force with solution frequency for mode 3 when mechanical damping is both included and excluded. At the natural frequency, the combined aerodynamic force is equal and opposite to any mechanical damping force. For solutions outside the natural frequency (including the resonant frequency), the resulting combined aerodynamic force is always non-zero and in phase with the blade motion, and hence this resultant force does not do any work. The only unique feature to be observed at resonance is the exactly 90° phase lag of the blade motion behind the excitation force. (Note that this exact phase relation is assumed by the decoupled method at the natural frequency.) Since only the combined force is available, the phase of the excitation force cannot be determined, hence, the response phase remains unknown. Outside the natural frequency, no deductions can be made from the combined force, which is nonzero in magnitude and always in phase with blade motion. Therefore, due to the lack of knowledge of the individual damping and excitation forces, a single coupled solution at a given excitation frequency cannot be used to predict the response for any other frequency.

4.6. Sensitivity to frequency shift

When choosing between a coupled or decoupled forced response analysis for a particular case, a consideration is the sensitivity to the added mass effect, which will determine the level of agreement between the coupled solution at the blade natural frequency and the resonant peak. A coupled solution at the natural frequency will provide a vibration amplitude close to the resonant peak for cases that are insensitive to frequency shift, whilst the more sensitive cases require resonance tracking. Whilst it has been shown that the frequency shift is caused by the inertial aerodynamic damping component, the sensitivity of the coupled solution to frequency shift depends on the sharpness of the resonant peak, which is determined by the overall system damping.

A generalized approach is presented to evaluate the accuracy in which a single coupled solution at the blade natural frequency approximates the resonant peak for cases subject to aerodynamic and mechanical damping. As shown in Eq. (12), the coupled solution can be emulated by considering both the inertial and viscous terms of the decoupled aerodynamic damping force, where the solution magnitude is given by

$$|\tilde{q}_c| = \frac{|\tilde{f}|}{\sqrt{(\omega_n^2 - m\omega^2 - d_n^{\text{real}})^2 + (2\zeta_{\text{mech}} m\omega_n\omega - d_n^{\text{imag}})^2}}. \tag{18}$$

The decoupled solution in Eq. (5) can be written in a similar manner, directly scaling only the viscous component of the aerodynamic damping force to provide an expression for the resonant peak amplitude, given by

$$|\tilde{q}_d| = \frac{|\tilde{f}|}{\sqrt{(\omega_n^2 - m\omega^2)^2 + (2\zeta_{\text{mech}} m\omega_n\omega - d_n^{\text{imag}})^2}}. \tag{19}$$

The validity of representing the resonant peak amplitude by the decoupled solution at the natural frequency was shown in Table 3. With forcing at the natural frequency and using unity modal mass, an expression for the accuracy of the coupled solution is given by the ratio of the coupled and decoupled solutions,

$$\frac{q_c}{q_d} = \frac{2\zeta_{\text{mech}}\omega_n^2 - d_n^{\text{real}}}{\sqrt{(d_n^{\text{real}})^2 + (2\zeta_{\text{mech}}\omega_n^2 - d_n^{\text{real}})^2}}. \tag{20}$$

Representing the aerodynamic damping force components in terms of phase as $d_n^{\text{real}} = d_n\cos\theta$ and $d_n^{\text{imag}} = d_n\sin\theta$, and taking r as the ratio of mechanical to aerodynamic damping

$$r = \frac{\zeta_{\text{mech}}}{\zeta_{\text{aero}}} \tag{21}$$

results in an expression for the accuracy of the coupled solution at the blade natural frequency in terms of the phase lag, $-\theta$, of the aerodynamic damping force:

$$\frac{q_c}{q_d} = \frac{(r+1)\sin(-\theta)}{\sqrt{[\cos(-\theta)]^2 + [(r+1)\sin(-\theta)]^2}}. \tag{22}$$

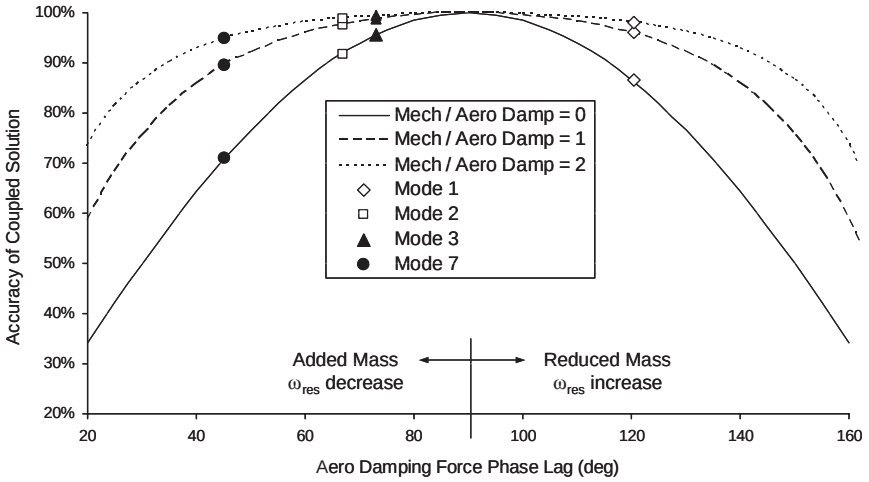

Fig. 14. Sensitivity of coupled solution at natural frequency to fluid–structure coupling effect.

As shown in Fig. 14, the agreement between the coupled solution and the resonant peak is determined exclusively by the phase of the aerodynamic damping force for any given level of mechanical damping. Included on the graph are the coupled solutions of four modes repeated with varying levels of mechanical damping. The coupled solution is insensitive to the frequency shift for cases with phase lag close to 90° where the inertial damping force component is small. Cases with a higher inertial component become more sensitive due to the increase in frequency shift. Mechanical damping plays an important role in the sensitivity to frequency shift by influencing the sharpness of the resonant peak. For cases subject to very low mechanical damping, the sensitivity is high, and the inclusion of mechanical damping can dramatically reduce the sensitivity of the system.

It is shown that the coupled solution at the natural frequency can predict the resonant peak with reasonable accuracy for cases with significantly high mechanical damping or when the aerodynamic damping force is known to be close to 90°. For example, the coupled solutions for the four modes predict the resonant peak with 95% accuracy when the mechanical damping ratio is set to be twice that of the aerodynamic damping. However, it has been shown that the phase of the aerodynamic damping force can vary significantly for each individual mode and the position any particular case on the graph cannot be determined without knowing the aerodynamic damping forces. Therefore, it can be dangerous to assume that a single coupled solution will accurately predict the resonant peak for cases where mechanical damping does not dominate.

Whilst mechanical damping prediction methods are immature, the work of Ning et al. (2003b), indicates that mechanical damping of typical compressor blades without friction dampers is greatly reduced for high-order modes, where blade motion is concentrated within the aerofoil. It can therefore be deduced that the sensitivity to frequency shift is likely to be high for bladerow interaction problems, where high-order modes result in low mechanical damping. It has been shown that the aerodynamic damping forces induced by high-order modes can produce high inertial components, which further highlights the potential for high sensitivity in such cases. It has been demonstrated that the coupled method can significantly under-predict the resonant peak when solved only at one frequency for any lightly-damped blade, with a particular emphasis on high-frequency bladerow interaction problems. The decoupled method has been shown to be insensitive to solution frequency for a range of frequency shifts that are likely to be encountered in typical cases of interest.

5. Conclusions

Two fully-coupled forced response methods have been developed with the intention of increasing computational efficiency over the decoupled method by combining the calculation of aerodynamic excitation and damping forces. Based on a highly efficient frequency-domain fluid solver with nonlinear capabilities, the modal equation is fully integrated into the flow solver and solved either directly in the frequency domain or by time-marching using a hybrid

approach. The coupled and decoupled solutions were obtained for three low order modes and one high order mode of the NASA Rotor 67 transonic aero fan. Blade excitation is given by hypothetical inlet distortions in order to provide a realistic test case that is typical of inlet distortion and bladerow interaction problems.

The coupled solutions were found to be strongly affected by a frequency shift due to a fluid–structure coupling effect, whereas the decoupled solution was shown to be insensitive to frequency shift. A novel closed-loop resonance tracking algorithm was incorporated into the coupled solution to adjust the solution frequency and obtain the peak vibration amplitude at the new resonant condition. Due the need for multiple solutions, the computational efficiency of the coupled solution showed no gain over the decoupled method. In contrast, the decoupled method is shown to be insensitive to frequency shift, maintaining resonance at the blade natural frequency and capturing the resonant peak with one solution.

A study into the fluid–structural coupling effect identified the source of the frequency shift in the coupled solution to be due to the added mass effect of the vibration-induced aerodynamic damping forces. A single coupled solution at any frequency cannot be used to predict resonance; hence coupled methods must rely on multiple solutions to find the resonant peak. The need for resonance tracking with coupled methods is especially important for high-frequency bladerow interaction problems, where low mechanical damping and strong fluid–structure coupling effects are likely to be encountered. The decoupled method is identified as the preferred approach to bladerow interaction problems due to the ability to accurately predict the resonant peak with high efficiency from a single solution.

Acknowledgements

This research is funded by the European Union Framework V R&D project "Development of Innovative Techniques for Compressor Aero-Mechanical Design (DITCAD)", Contract No. ENK5-CT-2000-00086.

References

Bell, D.L., He, L., 2000. Three-dimensional unsteady flow for an oscillating turbine blade and the influence of tip leakage. ASME Journal of Turbomachinery 122, 93–101 ASME 98-GT-571.

Bréard, C., Vahdati, M., Sayama, A.I., Imregun, M., 2000. An integrated time-domain aeroelasticity model for the prediction of fan forced response due to inlet distortion. ASME Paper 2000-GT-0373.

Campobasso, M.S., Giles, M.B., 2000. Flutter and forced response of mistuned turbomachinery. Report NA-00/20, Oxford University Computing Laboratory.

Chen, T., Vasanthakumar, P., He, L., 2001. Analysis of unsteady bladerow interaction using non-linear harmonic approach. AIAA Journal of Power and Propulsion 17 (3), 651–658.

Chiang, H.D., Kielb, R.E., 1993. An analysis system for blade forced response. ASME Journal of Turbomachinery 115, 762–770 ASME 92-GT-172.

Gerolymos, G.A., 1993. Coupled three-dimensional aeroelastic stability analysis of bladed disks. ASME Journal of Turbomachinery 115, 791–799.

Giles, M.B., 1992. An approach for multi-stage calculations incorporating unsteadiness. ASME Paper 92-GT-282.

Green, J.S., Marshall, J.G., 1999. Forced response prediction within the design process. Third European Conference on Turbomachinery, London, March 1999.

Hall, K.C., Clark, W.S., Lorence, C.B., 1994. A linerarized Euler analysis of unsteady transonic flows in turbomachinery. ASME Journal of Turbomachinery 116, 477–488.

Kielb, R.E., 1999. Forced response design analysis. VKI Lecture Series 1999–05, von Karman Institute for Fluid Dynamics, Belgium.

Li, H.D., He, L., 2002. Single-passage analysis of unsteady flows around vibrating blades of a transonic fan under inlet distortion. ASME Journal of Turbomachinery 124, 285–292 ASME 2001-GT-272.

Liu, B.-L., 1994. High frequency flow/structure interaction in dense subsonic fluids. NASA Contractor Report, SuDoc NAS 1.26:194007/NAS8-38187, Rockwell.

Manwaring, S.R., Kirkeng, K.L., 1997. Forced response vibrations of a low pressure turbine due to circumferential temperature distortions. In: Fransson, T.H. (Ed.), Eighth International Symposium on Unsteady Aerodynamics and Aeroelasticity of Turbomachines, Stockholm, 14–18 September 1997. Kluwer Academic Publishers, Dordrecht.

Marshall, J.G., 1996. Prediction of turbomachinery aeroelasticity effects using a 3D non-linear integrated method. Ph.D. Thesis, Imperial College of Science Technology and Medicine, University of London.

Marshall, J.G., Chew, J.W., Xu, L., Denton, J.D., 2000. Prediction of low engine order inlet distortion driven resonance in a low aspect ratio fan. ASME 2000-GT-0374 (May 2000).

Moffatt, S., He, L., 2003. Blade forced response prediction for industrial gas turbines. Part 1: Methodologies". ASME GT2003-38642.

Moyroud, N., Cosme, N., Jöker, M., Fransson, T.H., Lornage, D., Jacquet-Richardet, G., 2000. A fluid-structure interfacing technique for computational aeroelastic simulations. In: Ferrand, P., Aubert, S. (Eds.), The Ninth International Symposium, September 4–8, 2000, Presses Universitaires de Grenoble.

Ning, W., Li, Y.S., Wells, R.G., 2003a. Predicting bladerow interactions using a multistage time-linearized Navier–Stokes solver. ASME Journal of Turbomachinery 125, 25–32 ASME paper No. 2002-GT-30309.

Ning, W., Moffatt, S., Li, Y., Wells, R.G., 2003b. Blade forced response prediction for industrial gas turbines. Part 2: Verification and application. ASME GT2003-38642, 2003.

Sayama, A.I., Vahdati, M., Imregun, M., 2000. An integrated nonlinear approach for turbomachinery forced response prediction. Part 1: Formulation. Journal of Fluids and Structures 14, 87–101.

Schmitt, S., Nürnberger, D., Carstens, V., 2003. Evaluation of the principle of aerodynamic superposition in forced response calculations. Tenth International Symposium on Unsteady Aerodynamics and Aeroelasticity of Turbomachines Symposium, Duke University, Durham, NC, USA, 7–11 September 2003.

Silkowski, P.D., Rhie, C.M., Copeland, G.S., Eley, J.A., Bleeg, J.M., 2001. CFD investigation of aeromechanics. ASME Paper 2001-GT-0267.

Srivastava, R., Bakhle, T.G., Keith, T.G., Jr., 2002. Flutter analysis of a transonic fan. ASME Paper GT-2002-30319.

Tran, D.-M., Liauzun, C., Labaste, C., 2003. Methods of fluid-structure coupling in frequency and time domains using linearised aerodynamics for turbomachinery. Journal of Fluids and Structures 17, 1161–1180.

Vasanthakumar, P., Chen, T., He, Li., 2000. Three-dimensional viscous computation of blade flutter and forced response using nonlinear harmonic approach. In: Ferrand, P., Aubert, S. (Eds.), The Ninth International Symposium on Unsteady Aerodynamics and Aeroelasticity of Turbomachines, September 4–8, 2000, Presses Universitaires de Grenoble.

Further reading

Marshall, J.G., Giles, MB., 1997. Some applications of a time-linearized Euler method to flutter & forced response in turbomachinery. Proceedings of the Eighth International Symposium of Unsteady Aerodynamics and Aeroelasticity of Turbomachines, Stockholm, Sweden.